Ubr1 mediates conserved mitophagy

Ting Song[1], Xiuwen Fan[1], Siyao Wang[2], Yanxin Zhang[3], Fangkui Yin[2], Ke Wang[1], Haoxin Lun[2], Lekang Zhang[1], Wendi Zhang[1], Zhiyuan Hu[1], Yuying Wang[1], Ziqian Wang[1,*], Zhichao Zhang[1,*]

[1]Central Hospital of Dalian University of Technology, Faculty of Medicine, Dalian University of Technology, Dalian, Liaoning (China), 116024.

[2]Central Hospital of Dalian University of Technology, School of Chemistry, Dalian University of Technology, Dalian, Liaoning (China), 116024.

[3]School of Bioengineering, Dalian University of Technology, Dalian, Liaoning (China), 116024.

[*]Correspondence to: Zhichao Zhang, Email: zczhang@dlut.edu.cn; Ziqian Wang, Email: wangziqian@dlut.edu.cn

Highlights

1. Ubr1 mediates mitophagy in yeast with its evolutionary counterparts UBR1 and UBR2 acting independently and in parallel with Parkin in mammalian cells.

2. The C-terminus of Ubr1 directly binds to Hsp70 and the β-hairpin structure on mitochondrial proteins, and ubiquitinates a lysine residue located within the β-hairpin loop, thereby promoting ubiquitin-dependent mitophagy.

3. UBR1- and UBR2-mediated mitophagy offers novel therapeutic targets for mitophagy-associated diseases.

Abstract

Mitophagy is a selective autophagic process that controls mitochondrial homeostasis. Although Parkin has been identified as a mammalian E3 ubiquitin ligase for mitophagy, its homologues do not exist in yeast. Here, we demonstrate that E3 ligase Ubr1 mediates mitophagy in yeast with its evolutionary counterparts UBR1 and UBR2 (UBR1/2) acting independently and in parallel with Parkin in mammalian cells. The new function of Ubr1 ubiquitylating mitochondrial proteins via the non-N-end rule was identified. Structurally and mechanistically, with the assistance of Hsp70, the C-terminus of Ubr1 directly binds β-hairpin on mitochondrial proteins and ubiquitinates the lysine located within the β-hairpin loop, leading to autophagosomal protein LC3 recruitment to mitochondria. A physical complex of Hsp70-Ubr1-VDAC1 is required for Ubr1 translocation to the mitochondria and act there. The conservation of Ubr1 (UBR1/2) mediated mitophagy and the widespread expression of UBR1/2 in neuronal and cancer cells render them a more pivotal target than Parkin, especially since UBR1 overexpression provides stronger neuroprotection than Parkin in dopaminergic (DA) cells. The repurposing of antipsychotic drug clozapine in anti-triple negative breast cancer (TNBC) through UBR2 binding demonstrates that UBR1/2 are druggable targets for mitophagy-associated diseases.

Introduction

Mitophagy, an organelle-specific type of autophagy, has been developed to maintain mitochondrial quality control (QC)[1-4]. The best described E3 ligase connecting proteostasis with mitophagy is Parkin[5-7]. However, an increasing number of studies have shown the existence of alternative pathways, where different proteins can recruit autophagic machinery independently of Parkin[8]. For example, the removal of paternal mitochondria in pigs and rhesus monkeys is autophagy and ubiquitin-dependent, but Parkin-independent[9]. In *Saccharomyces cerevisiae* (baker's yeast), the ubiquitin protease Ubp3-Bre5 is specifically required for stress-induced mitophagy[10]. However, no Parkin is encoded in yeast, and the E3 ubiquitin ligase engaged in yeast mitophagy remains unidentified.

In yeast, the RING-type Ubr1 E3 ligase mediates not only the Arg/N-end rule pathway to ubiquitinate proteins through recognition of the N-terminal residues termed N-degrons[11,12], but also non-N-degrons such as CPY representing misfolded proteins[13], and Cup9, a transcriptional repressor[14,15]. Yeast Ubr1 has both sequential and functional homologs with mammalian UBR1 and UBR2 (abbreviated as UBR1/2), which together regulate the mammalian Arg/N-end rule pathway[16].

Ubr1 contains type-1 N-degrons, type-2 N-degrons, and other substrate-binding sites to interact with different proteins[12]. When Ubr1 mediates cytoplasmic protein QC, Hsp70 is required to detect misfolded proteins by an unclear mechanism[13,17]. Hsp70 is a conserved chaperone that not only assists Ubr1 in the ubiquitination process but is also essential for Parkin translocation under mitochondrial stress[18]. Our recent findings revealed that Hsp70 can facilitate parkin-mediated ubiquitination of mitophagy substrates[19]. However, no evidence has been found that Ubr1 functions in mitochondrial QC in either yeast or mammalian cells.

In this study, we identified a previously unknown role for Ubr1. Ubr1 mediates a highly conserved mitophagy pathway by directly ubiquitylating mitochondrial substrates VDAC1, and so on, following a non-N-end rule, leading to adaptor p62 and autophagosomal protein LC3 recruitment to mitochondria. The C-terminus of Ubr1 directly binds Hsp70, and the Hsp70-Ubr1 complex serves as a scaffold to specifically recognize the β-hairpin with a lysine located within the β-hairpin loop, which is shared by the mitochondrial ubiquitination substrates of Ubr1. The formation of Hsp70-Ubr1-VDAC ternary complex is the structural foundation underlying Ubr1-mediated ubiquitin-dependent mitophagy. We also revealed that UBR1-mediated mitophagy could offer a complementary target to counteract Parkinson's disease (PD) since UBR1 overexpression has stronger mitophagy induction and neuroprotective effects than Parkin in DA cells. Repurposing of the antipsychotic drug clozapine was found to enhance the anti-triple-negative breast cancer (TNBC) of doxorubicin through UBR2-mediated mitophagy inhibition *in vivo*.

Results

1. Cytosolic Ubr1 tranlocates to mitochondria and mediates the ubiquitin-dependent mitophagy pathway in yeast

We performed a multidimensional proteomics analysis to identify novel E3 ligases associated with the mitophagy machinery in yeast *S. cerevisiae* BY4741, as yeast do not encode Parkin. Mitophagy was induced by YPL-culture followed by nitrogen starvation (SD-N), and then subjected to four mitophagy assays: (1) degradation of ectopically expressed outer-membrane-targeted GFP (OM45-GFP, Supplementary Fig. 1a); (2) fluorescent colocalization of OM45-GFP and vacuole protein Vph1 (Supplementary Fig. 1 b); (3) transmission electron microscopy (TEM) finding double-membrane mitochondria inside vacuoles (Supplementary Fig. 1c); and (4) immunogold labeling of ubiquitin on mitochondria inside vacuoles (Fig. 1a). In response to starvation, wide-type (WT) yeast underwent mitochondrial ubiquitination followed by progressively OM45-GFP degradation, whereas deletion of the autophagosomal ubiquitin-like protein Atg8 (*ΔAtg8*) abolished both mitochondrial ubiquitination and OM45-GFP degradation (Supplementary Fig. 1a). Simultaneously, fluorescence microscopy revealed OM45-GFP colocalize with vacuoles (red, Supplementary Fig. 1b). TEM revealed the presence of double-membrane organelles inside vacuoles (Supplementary Fig. 1c), and immunogold labeling with an anti-ubiquitin antibody demonstrated that mitochondria sequestered inside vacuoles were decorated with substantially more gold particles than those residing in the cytosol (Fig. 1a). Collectively, these findings confirm that starvation efficiently induces ubiquitin-dependent mitophagy in yeast cultured in YPL medium, despite the absence of Parkin homologue in this organism.

Furthermore, SILAC-based ubiquitin remnant motif enrichment (K-ε-GG) was employed to characterize the mitochondrial ubiquitinome in yeast (Fig. 1b). Mass spectrometry identified 1719 ubiquitination sites distributed across 911 proteins that exhibited significantly elevated ubiquitination levels following 3 h of SD-N starvation. (fold change > 1.5, $p < 0.05$; Table S1). Overlapping of this dataset with the mitochondrial proteome (UniProt KB SL-0173) yielded a subset of candidate substrates, including POR1, SAM50, TOM40, DUG1, FZO1, GUT1, CIT1, ARG5,6, FUM1, COX8 and GPM1 (Fig. 1b). The ubiquitination and subsequent degradation of POR1 SAM50, and TOM40, the three top-ranked mitochondria proteins in the ubiquitinome, were validated by immunoprecipitation (Co-IP) and western blotting for a ladder of high molecular weight ubiquitinated proteins in wild-type yeast but were abrogated in ΔAtg8 mutants (Supplementary Fig. 1d-f). The ubiquitination of POR1, the VDAC1 homolog in yeast, was further verified to occur on mitochondria by co-IP and Western blotting on isolating yeast mitochondria (Fig. 1c). These substrates partially overlapped with those targeted by Parkin. Notably, POR1, the yeast homolog of the Parkin's classic substrate VDAC1, is top-ranked among the most prominently ubiquitinated mitochondrial proteins in our dataset, while TOM20, another well-characterized

substrate of Parkin-mediated mitophagy[20], showed no significant change in ubiquitination level (Supplementary Fig. 1g). This differential substrate profile implies the existence of an alternative E3 ligase.

To find the E3 ligase involved in yeast mitophagy, we immunoprecipitated POR1 using an anti-FLAG antibody from yeast cells starved for 3 h and identified the bound proteins by mass spectrometry (Fig. 1d and Table S2). Compared with non-starved yeast, 24 proteins were reproducibly and statistically significantly enriched. Among those, the Atg8-conjugation machinery (Atg8, Atg9 and Atg12) and the Atg8-binding autophagy receptor (Ede1 and End3)[21] were identified (green labeled, Fig. 1d). Our approach also got known mitophagy regulator Ubp3-Bre5 deubiquitination complex (red labeled, Fig. 1d). Importantly, also enriched in this sample were peptides corresponding to an E3 ligase Ubr1, as well as Ubc2 (also known as Rad6)[22], a Ubr1-binding E2 ubiquitin-conjugating enzyme (purple labeled, Fig. 1d). Ubr1 is the only E3 ligase in POR1 interactome. To confirm the IP-MS data, we co-expressed FLAG-POR1 along with HA-Ubr1 or Myc-Atg8. Co-IP assays consistently showed that FLAG-POR1 increasingly binds to Ubr1 and Atg8 under starvation (Supplementary Fig. 1h). Subcellular fractionation and western blotting assays showed that ~80% of HA-Ubr1 translocated from cytoplasm to mitochondria upon starvation (Fig. 1e).

The evidence that Ubr1 is involved in mitophagy was further supported by OM45-GFP cleavage and TEM assay under *Ubr1* deletion (Δ*Ubr1*), which strongly reduced mitophagy (Fig. 1 f and g). Δ*Ubr1* and Δ*Atg8* yeast cells could not grow on YPL plates, on which mitochondria-dependent respiration is essential for yeast growth, consistent with the contribution of Ubr1 in mitophagy (Supplementary Fig. 1i). The novel function of Ubr1 in mitophagy was unveiled here, which is beyond the scope of its known biological roles[23].

2. UBR1/2 mediates conserved ubiquitin-dependent mitophagy pathway in mammals

To determine whether the Ubr1-mediated mitophagy pathway is evolutionarily conserved across species, we examined the functional contribution of its human homologs, UBR1 and UBR2, to ubiquitin-dependent mitophagy in mammalian cells. Exposure of HEK293 cells to carbonyl cyanide *m*-chlorophenyl hydrazone (CCCP) induced a marked translocation of GFP-UBR1 to mitochondria, as evidenced by colocalization analysis (Fig. 2a). Moreover, shRNA-mediated knockdown of either *UBR1* or *UBR2* substantially attenuated CCCP-induced mitophagy, as quantified by the lysosomal delivery of matrix-targeted mKeima (Fig. 2b) and by the maintenance of the mitochondrial to nuclear DNA (mtDNA/nuDNA) ratio (Supplementary Fig. 2a). Consistent with these findings, *UBR1* or *UBR2* knockdown also impaired OAR inhibitor cocktail (oligomycin, antimycin A, and rotenone)-induced degradation of mitochondrial proteins, including COX IV, PDH, and TOM20 (Supplementary Fig. 2b), and resulted in the accumulation of swollen mitochondria with a concomitant defect in mitophagosome formation, as visualized by TEM (Fig. 2c), validating UBR1 and UBR2 serve as essential mediators of mitochondrial clearance.

Mechanistically, immunofluorescence analysis revealed that CCCP treatment promoted substantial colocalization of ubiquitin, the mitophagy adaptor p62, and the mitochondrial matrix protein PDH, a spatial convergence that was markedly diminished upon *UBR1* or *UBR2* depletion (Fig. 2d). Furthermore, whereas overexpression of wild-type UBR1 potentiated CCCP-induced degradation of COX IV, overexpression of the catalytically inactive UBR1 C1220S RING domain mutant failed to elicit a similar effect, confirming that the E3 ubiquitin ligase activity of UBR1 is requisite for its mitophagy function (Supplementary Fig. 2c). Collectively, these data confirmed that the Ubr1-mediated mitophagy pathway is functionally conserved from yeast to mammals, wherein UBR1 and UBR2 serve as essential E3 ligase to induce ubiquitin-dependent mitophagy.

3. β-hairpin with a loop-located lysine mediates Hsp70-UBR1/2-substrates interaction and determines mitochondrial ubiquitination in mitophagy

We next sought to elucidate the mechanism governing the mitochondrial translocation of Ubr1/UBR1/UBR2 and the consequent induction of mitochondrial ubiquitination and mitophagy. The four top-ranked mitophagy substrate candidates, POR1/VDAC1, SAM50, TOM40, and DUG1, share a β-hairpin motif, within which a unifying lysine located at the loop between two β-strands undergoes ubiquitination upon starvation (Table S1 and Supplementary Fig. 3a). Therefore, we synthesized the two peptides derived from the β-hairpin of human VDAC1 *in vitro*, either stabilized by a disulfide bond to retain the β-hairpin conformation or not, named as Cyclic β-hairpin and Linear β-hairpin (Fig. 3a). Isothermal titration calorimetry (ITC) assays showed that the Cyclic β-hairpin retained the binding affinity of VDAC1 to Ubr1 (K_d = 7.58 μM vs 11.42 μM), whereas the Linear β-hairpin peptide exhibited no detectable binding to Ubr1 (Fig. 3a and Supplementary Fig. 3b). Moreover, the Cyclic β-hairpin, but not the Linear variant, blocked CCCP-induced GFP-UBR1 translocation to mitochondria, mitophagy, and subsequent cell death in HEK293 cells (Fig. 3b and Supplementary Fig. 3c and 3d). Collectively, these findings establish that the β-hairpin motif serves as a critical recognition determinant for Ubr1/UBR1/UBR2-engaged mitophagy.

Furthermore, we constructed fusion proteins in which the β-hairpin motif of VDAC1, or control peptides, was fused to the C-terminus of TOM20. Immunoprecipitation of TOM20 from HA-UBR1-transfected HEK293 cells revealed that, in contrast to TOM20 fused with control peptides, TOM20 fused with this β-hairpin acquired the capacity to interact with HA-UBR1 and undergo ubiquitination (Fig. 3c). Thus, the β-hairpin alone suffices to convert a non-substrate protein into a Ubr1/UBR1/UBR2-induced mitophagy substrate, validating this motif as the critical recognition determinant of Ubr1/UBR1/UBR2-induced mitophagy.

Given that the POR1's interactome analysis identified peptides corresponding to the Hsp70 isoforms Ssa1, Ssa2, and Ssa3, along with their cochaperones Sse1 (Hsp110), Hsp104, and Hsp26 (highlighted in blue, Fig. 1b), we further hypothesized that Ubr1-

mediated ubiquitination of mitochondrial substrates is dependent on Hsp70 activity. Notably, pharmacological inhibition of Hsp70 by well-characterized inhibitors, **VER-1550008**[24], **S1g-10**[25], and **MKT-077**[26], significantly blocked CCCP-induced mitochondrial translocation of UBR1/2, UBR1/2-VDAC1 interaction, and VDAC1 ubiquitination (Supplementary Fig. 3e and Fig. 3d). A similar phenomenon was observed for SAM50 and TOM40 (Supplementary Fig. 3f and 3g). Moreover, pull-down assay with anti-FLAG affinity beads showed addition of Hsp70 significantly increased the amounts of VDAC1 associated with FLAG-Ubr1 (Fig. 3e). ITC and biolayer interferometry assays with recombinant-expressed proteins further validated that Hsp70 potently binds to Ubr1 (K_d = 0.95 and 0.78 μM) (Fig. 3a, Supplementary Fig. 3h and 3i), and the Hsp70-Ubr1 complex binds to VDAC1 with a 10-fold higher affinity than that of Ubr1 alone (K_d = 0.38 μM vs 11.42 μM) (Fig. 3a, Supplementary Fig. 3h and 3b). Notably, the binding isotherm of VDAC1 into Hsp70-Ubr1 complex conformed to a single-site binding model (N ≈ 0.95, Supplementary Fig. 3h), indicating that the Hsp70-Ubr1 complex functions as a cooperative scaffold that facilitates high-affinity recognition of the mitochondrial substrate VDAC1. Collectively, these data demonstrate that Hsp70 serves as an obligate cofactor of Ubr1/UBR1/UBR2 to recognize and ubiquitinate mitochondrial membrane targets and initiate mitophagy.

STUB1 is another E3 ligase serving as the co-chaperone of Hsp70 and exhibits similar binding affinity with Ubr1. A well-known substrate of Hsp70-STUB1 complex for ubiquitination-proteasomal degradation[27], AR-V7, was tested to verify the specificity of the Hsp70-UBR1 complex recognition. Overexpression of UBR1 did not affect AR-V7 protein level, whereas STUB1 significantly suppressed AR-V7 level, consistent with previous reports (Supplementary Fig. 3j). We also tested whether Hsp90 is involved in the Hsp70-UBR1-VDAC1 complex. Hsp90 inhibitors did not affect UBR1 translocation (Supplementary Fig. 3k), excluding its participation.

4. The previously unrecognized C-terminus of Ubr1/UBR1/UBR2 mediates Hsp70-UBR1/2-substrates interaction and determines mitochondrial ubiquitination in mitophagy

We next performed a domain mapping assay to delineate the region of UBR1 responsible for mitochondrial substrate recognition and Hsp70 engagement. The C-terminal fragment of UBR1 (residues 1380-1749) bound both VDAC1 and Hsp70 with an affinity comparable to that of the full-length protein, whereas the N-terminal fragment (residues 1-1209) exhibited no detectable interaction with either partner (Fig. 4a-c), demonstrating the previously uncharacterized C-terminal region of UBR1 as the minimal module sufficient for assembly of the ternary Hsp70-UBR1-VDAC1 complex. Protein-protein interaction simulations performed with AlphaFold 3 predicted that the β-hairpin motif of VDAC1 docks into a hydrophobic groove within the CHD domain of UBR1, delineated by residues Ser1427, Ser1431, His1435, Phe1438, and additional surrounding amino acids (Supplementary Fig. 4a). Consistent with this prediction, alanine mutation of these four residues (S1427A/S1431A/H1435A/F1438A, designated

UBR1^{4A}) markedly perturbed formation of the Hsp70-UBR1-VDAC1 complex in pull-down assays (Fig. 4 b-e). Functionally, UBR1^{4A} failed to translocate to mitochondria upon CCCP treatment and was unable to restore mitophagy or rescue cell death in UBR1-deficient HEK293 cells (Fig. 4 f and g, Supplementary Fig. 4b). In contrast, mutations in the canonical substrate-binding sites, Box1 (V122L) and Box2 (N232A)[28], rescued mitophagy and cell death as efficiently as wild-type UBR1 (Fig. 4f and Supplementary Fig. 4b). Additionally, UBR1^{4A} had no appreciable effect on the ubiquitination and degradation of RGS4-His, a well-established N-end rule substrate of UBR1, whereas UBR1^{V122L} significantly perturbed this process (Supplementary Fig. 4c).

Collectively, these findings demonstrate that, under mitophagy-inducing conditions, UBR1 recognizes and ubiquitinates mitochondrial substrates through a novel substrate recognition rule that is mechanistically distinct from the classical N-end rule, wherein the functionally uncharacterized C-terminal domain of UBR1 serves as the critical recognition module. Consistent with this conclusion, FLAG-VDAC1 bearing an intact N-terminus was robustly ubiquitinated by UBR1 upon CCCP treatment in HEK293 cells, accompanied by the recruitment of both p62 and LC3 (Fig. 4h).

5. UBR1 is independent of Parkin and has stronger mitophagy induction and neuroprotective effects than Parkin

We investigated UBR1-mediated mitophagy in the protection of human neuronal cells. Dopaminergic SH-SY5Y cells with high UBR1 expression were analyzed (Supplementary Fig. 5a). As shown in Fig. 5a, treatment of SH-SY5Y cells with complex I inhibitor/parkinsonian neurotoxin methylpyridinium ion (MPP^+)[29] induced translocation of transfected GFP-UBR1 from the cytoplasm (0 h of MPP^+) to mitochondria (3 h of MPP^+), followed by final clearance of mitochondria (12 h of MPP^+), which is as similar as cells transfected GFP-Parkin (Fig. 5b). However, endogenous UBR1 induces significantly more mitophagy than Parkin as measured by mKeima fluorescent assay in SH-SY5Y cells knocking out *Parkin* or *UBR1* (Fig. 5c, 25.7 vs 42.5). Of note, double knockdown of *UBR1* and *Parkin* showed an additive mitophagy inhibition compared to the knockdown of *UBR1* or *Parkin* alone (Fig. 5d) under CCCP treatment. Thus, UBR1 seems to play a more critical role than Parkin and act independently in parallel ways to converge on mitophagy promotion.

More robust UBR1-induced mitophagy results in stronger neuroprotective effects than Parkin. As determined by the CCK-8 assay, UBR1 overexpression significantly ameliorated MPP^+-induced cell death in SH-SY5Y cells, resulting in significantly higher cell viability than Parkin overexpression (Supplementary Fig. 5b). Overexpression of UBR1, but not PINK1, reverses the MPP^+-induced cell death by *Parkin* knockdown (Supplementary Fig. 5c), further confirming UBR1 act independently in parallel with Parkin.

6. Clozapine enhances the anti-triple-negative breast cancer (TNBC)

of doxorubicin through UBR2-mediated mitophagy inhibition

To explore whether UBR1/2-mediated mitophagy is crucial for cancer chemoresistance, we focused on breast cancer because significantly higher *UBR2* mRNA levels have been found in breast carcinomas compared to healthy breast tissue, especially in TNBC cells[30]. Our western blotting assay in 7 breast cancer cell lines confirmed it. The highest UBR2 expression is in MDA-MB-231, whereas UBR1 is less expressed (Fig. 6a).

Treatment of MDA-MB-231 cells with 3 h of doxorubicin (DOX) led to an increase in Hsp70 and VDAC1 in UBR2 immunoprecipitants (lane 4 vs lane 3, Fig. 6b). VDAC1 ubiquitination occurred, followed by mitophagy at 24 h (lane 2 vs lane 1, Fig. 6c). Knockdown of *UBR2* inhibited DOX-induced mitophagy (lane 3 vs lane 2, Fig. 6c). TEM analysis revealed that the number of mitophagosomes was markedly decreased by *UBR2* knockdown, along with more swollen mitochondria with disrupted cristae (Supplementary Fig. 6a). As such, UBR2 mediates DOX-induced mitophagy in TNBC cells. Consistent with the established knowledge that mitophagy results in DOX resistance in breast cancer cells, *UBR2* knockdown sensitized cells to DOX (Fig. 6d).

To examine the therapeutic potential of targeting UBR2-mediated mitophagy, we tested whether the UBR1/2 inhibitor clozapine (CLZ)[31], an antipsychotic drug, could overcome DOX resistance. Our CETSA assay results showed that the thermal stability of UBR2 in MDA-MB-231 cell lysates with CLZ, but not the other two antipsychotic drugs, was significantly increased, confirming the *in situ* UBR2 inhibition of clozapine (Fig. 6e and Supplementary Fig. 6b). Indeed, CLZ treatment significantly inhibited DOX-induced mitophagy, closely mimicking the effects of *UBR2* knockdown (Supplementary Fig. 6c). We next observed the fate of MDA-MB-231 upon CLZ combined with DOX. Although CLZ alone did not affect cell viability, it significantly enhanced the effect of DOX on MDA-MB-231 (Fig. 6g). Importantly, treatment with CLZ and DOX in *UBR2* or *ATG7* knockdown MDA-MB-231 had no additive effects (Fig. 6g), confirming a UBR2-dependent and autophagy-dependent effect of CLZ. Compared to CLZ, neither olanzapine nor risperidone could enhance the effect of DOX (Supplementary Fig. 6d).

To evaluate CLZ in combination with DOX *in vivo*, MDA-MB-231 cells were injected into mice to induce subcutaneous xenograft tumors, followed by treatment with DOX (5 mg/kg) and DOX+CLZ (5 mg/kg + 10 mg/kg), respectively. As shown in Fig. 6h, DOX alone treatment reduced tumor volume after 21 days, consistent with previous reports. The combinational treatment of DOX and CLZ caused significantly stronger inhibition in tumor volume compared with DOX alone (Fig. 6h) without causing weight loss in mice (Supplementary Fig. 6e). Western blotting 36of COX IV, PDH, and TOM20 in isolated tumor tissues showed that DOX induced mitophagy, while combination with CLZ reversed these events, demonstrating the mitophagy inhibition effect of CLZ *in vivo* (Fig. 6i). Together, these results demonstrate that CLZ-mediated UBR2 inhibition combined with DOX can improve chemotherapy efficacy against TNBC through mitophagy inhibition.

Discussion

Thus far, the E3 ubiquitin ligases responsible for mediating ubiquitin-dependent mitophagy in yeast are still to be identified[32]. The effects of exogenously expressed Parkin in baker's yeast[33] suggest the existence of a mitophagy pathway. However, the lack of Parkin homology in yeast makes it impossible to trace this pathway essential for mitochondrial homeostasis. Here, we provide the first evidence that yeast Ubr1 is the evolutionary ortholog of its mammalian counterparts UBR1/2 to mediate a universal mitophagy pathway.

The classic function of cytosolic Ubr1/UBR1/UBR2 mediates cytoplasmic protein QC by ubiquitinating N-degrons via the N-end rule[23], as well as misfolded cytoplasmic proteins via an Hsp70-dependent, non-N-end rule[13]. What we found in this study is distinguished from the two mechanisms. Ubr1 translocates to mitochondria to specifically ubiquitylate certain mitochondrial proteins, thereby promoting mitophagy. From a structural perspective, the C-terminus of Ubr1 (human UBR1 residues 1380-1749) provides a binding site for Hsp70 and VDAC, which is separated from the N-degrons binding sites[12] and that for non-N-degron CUP9[15] and Plin2[34]. FLAG-VDAC1 with an intact N-terminus also interacts with and is ubiquitinated by Ubr1. From a functional perspective, Box1 or Box2 domain mutation of Ubr1 exhibit unaffected mitophagy-inducing activity under stress. As such, the ubiquitination of mitochondrial proteins by Ubr1 is independently of N-end rule. Although Ubr1-mediated misfolded protein degradation is also through non-N-end rule and requires Hsp70, the scope of substrate is different from that of Ubr1-mediated mitophagy. We showed that, biochemically, Ubr1-mediated mitophagy is substrate-specific. The formation of a ternary complex between Hsp70, Ubr1, and VDAC1 is the molecular basis by which Hsp70 assists Ubr1 in ubiquitinating mitochondrial substrates. It is the Hsp70-Ubr1 complex that binds VDAC1, by which Ubr1 moves to the mitochondria and ubiquitylates VDAC1 there. The β-hairpin structure on VDAC1 is the core motif, as it binds the Hsp70-Ubr1 complex as tightly as VDAC1 *in vitro* and inhibits UBR1 translocation to the mitochondria, thereby initiating mitophagy *in situ*. The β-hairpin with a loop-located lysine is a hallmark structural feature of mitophagy substrate proteins, rather than universal misfolded proteins that could be recruited by either Hsp70 or Ubr1. All the mitochondrial ubiquitination substrates revealed by ubiquitinome bear a β-hairpin with a lysine. The β-hairpin is then a hot spot for the future mitophagy inhibitor design.

UBR1/2 and Parkin act independently in parallel ways to converge on mitophagy promotion, since they can rescue the functional defects caused by the deficiency of each other and exert additive functional effects. Moreover, overexpression of UBR1/2 exhibit stronger protective effects than Parkin in neuronal cells. So far, about 30 causative genes for PD, including Parkin, which exhibit the highest frequency of mutation in PD patients, can only explain a small proportion of the etiology of PD[35]. UBR1/2 is emerging as a potential etiology of PD. A genetic association study supported the concept that rare variants in *UBR1* were significantly enriched in patients with 695 early-onset PD (EOPD)[36]. Regarding PD therapies, UBR1/2 could serve as potential therapeutic targets, either with *Parkin* mutant or intact.

UBR1/2 play roles in tissues beyond neural tissues. Unlike Parkin, which is lowly expressed or absent in most cancers, UBR1/2 are widely expressed in cancer tissues. A genome-wide siRNA lethality screening in cancer cell lines found that UBR2 stood out as the best protector of chemotherapy-induced cell death among the E3 ligases[30]. It was puzzling before the present discovery. Our study uncovers an unexpected mechanism involving UBR2-mediated mitophagy in DOX-resistant TNBC cell lines and *in vivo* models, particularly validated with the aid of the antipsychotic drug CLZ. CLZ is one of the few UBR1/2 inhibitors, and it was presumed to be an Arg/N-degron pathway inhibitor[31]. In this study, CLZ exhibited direct UBR2 binding in TNBC cells and enhanced the anti-TNBC activity of DOX through UBR2-dependent mitophagy inhibition *in vivo*. The UBR2 is then a druggable target for chemo-resistant TNBC, and likely the other chemo-resistant cancers, depending on mitophagy. In the meantime, CLZ presents a therapeutic strategy of repurposing old drugs for new uses, facilitating its entry into clinical trials for cancer, particularly in the absence of UBR1/2 inhibitors under development so far.

The mechanism-based anti-TNBC of CLZ could advance research on the druggability of UBR1/2 and the molecular druggability of their inhibitors. The binding mode of CLZ on UBR1/2 could guide the rational design of a new type of mitophagy regulator. Given our finding that UBR1/2 mediates mitophagy independently of its Box1 and Box2 (also known as the N-recognin sites), CLZ doesn't bind with UBR1/2's N-recognin sites, which is contrary to earlier work concerning CLZ's binding with UBR1/2[31]. Further studies are meaningful to uncover the direct binding sites of CLZ on UBR1/2, which could provide novel compounds acting on the UBR1/2-mediated mitophagy pathway in cancer.

Together, we found that an evolutionarily conserved Ubr1/UBR1/UBR2-mediated pathway regulates mitophagy and then maintains cell survival. It fills the gap in cross-species mitochondrial hemostasis. The identification of the new E3 ligase target is a breakthrough since mitochondrial homeostasis imbalance serves as a unifying mechanism underlying the multisystemic manifestations of various diseases. Excitingly, its druggability was identified by the mechanism-based anti-TNBC of CLZ through UBR2-mediated mitophagy. It opens numerous new doors for basic and clinical purposes.

Figure Legends

Fig.1 Ubr1 mediates mitophagy in yeast cells upon starvation.

a, Yeast cells were cultured in YPL for 12 h and then starved for 6 h, followed by immunogold labeling with an anti-ubiquitin antibody and examined by transmission electron microscopy (TEM). m, mitochondrion, v, vacuole, Scale bars, 1 μm. Ubiquitin-conjugated mitochondrion inside the vacuole (v) is indicated by red arrowheads, and those outside the vacuole is indicated by green arrowheads. **b**, Yeast cells were cultured in YPL for 12 h and then starved for 0 or 3 h. Top: A flowchart illustrating the process to quantify the ubiquitinome of starved yeast. Bottom: Rank order plot showing the proteins increasingly ubiquitinated ($\log_2$ ratios) between yeast cells treated with SD-N for 0 and 3 h. Values above the black dotted line ($\log_2$(fold change) > 0.58) were significantly ubiquitinated proteins upon starvation and are shown in red. **c**, Δ*Atg8* yeast

cells transfected with FLAG-POR1 were cultured in YPL for 12 h and then starved for 0, 3, 6 or 12 h. Mitochondria were isolated and subjected to co-IP with anti-FLAG antibody and western blotting with anti-ubiquitin antibody. **d**, Left: A flowchart illustrating the process of identifying POR1-interacting proteins upon starvation. Right: Volcano plot displaying the mass spectrometry results of FLAG pull-downs from yeast expressing FLAG-tagged POR1 starved for 0 or 3 h. 24 proteins that were significantly enriched (x axis; fold change > 1.5, y axis; *P* value < 0.05) are shown in red triangle. **e**, HA-Ubr1 transfected yeast cells were starved for 0 or 3 h. Mitochondria were isolated and subjected to western blotting with anti-HA antibody. Western blot of subcellular fraction probed with antibodies for cytosolic protein PGK and mitochondrial protein POR1. **f**, WT, Δ*Atg8,* or Δ*Ubr1* yeast cells stably expressing OM45-GFP were cultured in YPL and then starved for 6 h. Cells were analyzed for mitophagy via western blot by detecting GFP fusion protein cleavage. **g**, TEM of WT or Δ*Ubr1* yeast cells after starvation for 6 h. Scale bars, 1 μm. Mitochondria within and out of the vacuoles are indicated by red and green arrowheads, respectively. Data are expressed as mean ± s.d. (n = 3 biological replicates). Unpaired t-test was performed for **a**, **e** and **g**, $^{**}P < 0.01$. The data presented in **a**, **c**, **e-g** are representative of three independent experiments.

Fig.2 UBR1/2 mediates mitophagy in HEK293 cells upon CCCP treatment.

a, HEK293 cells co-transfected GFP-UBR1 with mitochondrial-targeted COX8-mCherry were treated with 20 μM CCCP for 3 h. Images of cells were obtained using confocal microscopy (scale bar, 5 μm). **b**, HEK293 cells stably expressing matrix-targeted mKeima were transduced with lentiviral control shRNA or shRNA targeting *ATG12*, *UBR1* or *UBR2*. Two independent shRNA sequences for each of UBR1 and UBR2 were applied as *UBR1-1*, *UBR1-2*, and *UBR2-1*, *UBR2-2*. Then, cells were treated with 20 μM CCCP for 12 h, followed by flow cytometry for mKeima. **c**, Control shRNA, *UBR1&UBR2* shRNA-transfected HEK293 cells were treated with 20 μM CCCP in combination with 200 nM BafA1 for 6 h, and then TEM was used to visualize the mitochondrial ultrastructure (scale bar, 5 μm). Red arrowheads indicate mitophagosomes. The yellow stars indicate the structure of mitochondrial crista. The swollen mitochondria without cristae are indicated by purple arrowheads. **d**, Confocal microscopy of control shRNA or *UBR1&UBR2* shRNA-transfected HEK293 cells upon 20 μM CCCP treatment for 3 h, using antibodies to p62 and PDH along with ubiquitin (scale bar, 5 μm). One-way ANOVA test was performed for **b**, and unpaired t-test was performed for **c**. $^{**}P < 0.01$. The data presented in **a-d** are representative of three independent experiments.

Fig.3 β-hairpin with a loop-located lysine underlies Hsp70-Ubr1-VDAC1 ternary complex and UBR1/2-mediated mitophagy.

a, The spatial positions of the ubiquitinated lysine (K266, corresponding to K267 in yeast homolog POR1) and the β-hairpin strand (green) in human VDAC1 (PDB 2JK4). Schemes of the two synthesized peptides. Residues correspond to that of VDAC1. The binding affinities between purified recombinant proteins or synthesized β-hairpin peptides derived from ITC or BLI assay were shown. **b**, HEK293 cells co-transfected with GFP-UBR1 and COX8-mCherry were treated with 20 μM CCCP for 3 h in the absence or presence of 10 μM β-hairpin peptides. Images of cells were obtained using

confocal microscopy (scale bar, 5 μm).**c**, HEK293 cells co-transfected HA-UBR1 with FLAG-TOM20-control peptide or FLAG-TOM20-β-hairpin were treated with 20 μM CCCP for 3 h followed by co-IP assay using anti-FLAG antibody and western blotting for a ladder of high molecular weight ubiquitinated TOM20 with anti-FLAG antibody, and for UBR1 with anti-HA antibody. **d,** HEK293 cells transfected with FLAG-VDAC1 were treated with 20 μM CCCP for 3 h in the absence or presence of 5 μM VER-155008, 2 μM S1g-10, or 5 μM MKT-077. Cell lysates were immunoprecipitated using anti-FLAG antibody and western blotting with anti-UBR1 and anti-UBR2 antibodies, and for a ladder of high molecular weight ubiquitinated FLAG-VDAC1 with anti-FLAG antibody. **e**, *in vitro* pull-down assays with anti-FLAG affinity beads were performed using purified FLAG-tagged Ubr1, Hsp70 and VDAC1. Protein samples were separated by SDS-PAGE and visualized using Coomassie blue staining. Data are expressed as mean ± s.d. (n = 3 biological replicates). One-way ANOVA test was performed for **b**, $^{**}P < 0.01$, ns indicates no significance. The data presented in **a-e** are representative of three independent experiments.

Fig. 4 C-terminus of Ubr1/UBR1/UBR2 mediates Hsp70-UBR1/2-substrates interaction and determines mitochondrial ubiquitination in mitophagy.

a, Summary of the binding ability of VDAC1 and Hsp70 to full-length, truncated or mutated UBR1. Amino acid positions for truncation or mutation are shown as indicated. **b, c**, HEK293T cells co-transfected HA-tagged truncated UBR1, full-length UBR1, or $UBR1^{4A}$ mutant with FLAG-tagged VDAC1 (**b**) or Myc-tagged Hsp70 (**c**) were treated with 20 μM CCCP for 3 h followed by co-IP assay with anti-FLAG antibody or anti-Myc antibody and western blotting for HA. **d**, HEK293T cells transfected with $UBR1^{WT}$ or $UBR1^{4A}$ were treated with 20 μM CCCP for 3 h followed by co-IP assay with anti-HA antibody and western blotting for endogenous Hsp70 and VDAC1 respectively. **e,** Schematic of UBR1 mutations. **f**, HEK293 or *UBR1* knockout (KO) HEK293 cells transfected with $UBR1^{WT}$, $UBR1^{V122L}$, $UBR1^{N232A}$ or $UBR1^{4A}$ were treated with 20 μM CCCP for 12 h followed by flow cytometry for mKeima. **g**, HEK293 cells co-transfected GFP-$UBR1^{WT}$ or GFP-$UBR1^{4A}$ with COX8-mCherry were treated with 20 μM CCCP for 3 h. Images of cells were obtained using confocal microscopy (scale bar, 5 μm). **h**, HEK293 cells transfected with FLAG-VDAC1 alone or co-transfected with HA-UBR1 were treated with 10 μM CCCP for 3 h. Cell lysates were immunoprecipitated using anti-FLAG antibody and western blotting for a ladder of high molecular weight ubiquitinated VDAC1 with anti-FLAG antibody, and for p62 and LC3 with respective specific antibodies. Data are expressed as mean ± s.d. (n = 3 biological replicates). One-way ANOVA test was performed for **f**. $^{**}P < 0.01$, ns indicates no significance. The data presented in **b-d, g** and **h** are representative of three independent experiments.

Fig. 5 UBR1 promotes mitophagy independently of Parkin and provides stronger protection of neuronal cells through mitophagy than Parkin.

a, b, SH-SY5Y cells stably expressing COX8-mCherry were transfected to transiently express GFP-UBR1 (**a**) or GFP-Parkin (**b**) and then treated with 200 μM MPP^+ for 3 or 12 h.The images of cells were obtained using confocal microscopy (scale bar, 20 μm). **c.** *UBR1* KO or *Parkin* KO SH-SY5Y cells that stably express mKeima were treated

with 200 μM MPP^+ for 12 h, followed by flow cytometry for mKeima. **d**. SH-SY5Y cells transduced with lentiviral control shRNA, *Parkin* shRNA, *UBR1* shRNA alone or in combination were treated with 10 μM CCCP for 24 h followed by western blotting for mitochondrial proteins COX IV, PDH and TOM20. Data are expressed as mean ± s.d. (n = 3 biological replicates). One-way ANOVA test was performed for **c** and **d**. $^{**}P < 0.01$, $^{*}P < 0.05$. The data presented in **a-d** are representative of three independent experiments.

Fig. 6 UBR2 inhibitor CLZ enhances DOX activity in TNBC cell lines and *in vivo* through mitophagy inhibition.

a, Western blot analysis of UBR1 and UBR2 in the indicated cell lines. **b,** MDA-MB-231 cells were treated with 0.5 μM DOX for 3 h. Cell lysates were subjected to western blotting for UBR2, Hsp70, and VDAC1 (Lane 1 and 2), or co-IP with anti-UBR2 antibodies and western blotting for UBR2 and Hsp70 antibody, and for a ladder of high molecular weight ubiquitinated VDAC1 with anti-VDAC1 antibody (Lane 3 and 4). **c**, MDA-MB-231 cells transduced with lentiviral control shRNA or *UBR2* shRNA were treated with 0.5 μM DOX for 24 h, followed by western blotting for COX IV and PDH. **d**, MDA-MB-231 cells transduced with lentiviral control shRNA or *UBR2* shRNA were treated with the indicated concentration of DOX for 48 h, followed by CCK-8 assays. **e**, MDA-MB-231 cell lysates were incubated with 10 μM CLZ at 37 ℃ for 2 h for each sample, and then subjected to heat at the indicated temperature for 3 min, followed by western blotting for UBR2 and Tubulin. The chemical structure of CLZ was shown. **f**, MDA-MB-231 cells were treated with the indicated concentration of DOX alone or in combination with 10 μM CLZ for 48 h, followed by CCK-8 assays. **g**, MDA-MB-231 transduced with lentiviral control shRNA, *UBR2* shRNA, or *ATG7* shRNA were treated with 0.2 μM DOX alone or in combination with 10 μM CLZ for 48 h, followed by CCK-8 assays. **h**, MDA-MB-231 cells were subcutaneously transplanted into nude mice, followed by treatment with vehicle, 5 mg/kg DOX alone, or in combination with 10 mg/kg CLZ. Mice were sacrificed on day 21, and tumors were excised as shown in the left. The tumor weight of each mouse in each group (n=7) is shown on the right. **i**, Western blot analysis of COX IV, PDH and TOM20 in the tumors excised from mice after treatment. Data are expressed as mean ± s.d. (n = 3 biological replicates). Two-way ANOVA test was performed for **f-h**, and one-way ANOVA test was performed for **i**. $^{**}P < 0.01$, $^{*}P < 0.05$. ns indicates no significance. The data presented in **a-c**, **e** and **i** are representative of three independent experiments.

Fig. 7 a, Model of Hsp70-Ubr1-VDAC1 complex that drives mitochondrial ubiquitination to recruit p62 and LC3. **b**, Ubr1 mediates mitophagy in yeast. In mammalian cells, UBR1/2 and Parkin mediate mitophagy independently of one another.

Acknowledgements

We thank professor L. K. Sun at the Norman Bethune Health Science Center of Jilin University for advices on experimental design and manuscript preparation. This study was supported by the National Natural Science Foundation of China (82270186 and 82273778), the Fundamental Research Funds for the Central University (DUT25YG250), and the Dalian City Life and Health Guidance Plan Project (2024ZDJH01PT012).

Author contributions

Conceptualization, T.S., Z.W. and Z.Z.; data curation, T.S., Z.W. and Z.Z.; methodology, T.S., Z.W. and Z.Z.; investigation: yeast cell experiments, T.S., Y.W., Y. Z. and H. L.; Western blotting and co-immunoprecipitation, X.F., K.W. and Z. H.; Protein purification, Y, Z., L. Z., W. Z. and H.L.; BLI and ITC assay, S. W. and F. Y.; bioinformatic analysis, F. Y. and Z. H; confocal imaging; X. F. and K.W.; writing-original draft preparation, T.S. and Z.Z.; writing-review and editing, T.S., Z.W. and Z.Z.; funding acquisition, T.S., Z.W., and Z.Z. All the authors have read and agreed to the published version of the article. All authors read and approved the final article.

Competing interests

The authors declare no competing interests.

Data availability

All data supporting the findings of this study are available in the article and its Supplementary Information. The MS data are provided with this paper as Table S1 and Table S1.

References

1. Onishi, M., Yamano, K., Sato, M., et al. (2021). Molecular mechanisms and physiological functions of mitophagy. EMBO J. 40, e104705.
2. Picca, A., Guerra, F., Calvani, R., et al. (2023). Mitophagy in human health, ageing and disease. Nat. Metab. 5, 2047-2061.
3. Ji, C.H. and Kwon, Y.T. (2017). Crosstalk and interplay between the ubiquitin-proteasome system and autophagy. Mol. Cells. 40, 441-449.
4. Varshavsky, A. (2017). The ubiquitin system, autophagy, and regulated protein degradation. Annu. Rev. Biochem. 86, 123-128.
5. Eiyama, A., Sakamaki, J.I. and Mizushima, N. (2024). The role of PINK1-Parkin in mitochondrial quality control. Nat. Cell Biol. 26, 1639-1651.
6. Wang, X.L., Feng, S.T., Wang, Z.Z., et al. (2021). Parkin, an E3 Ubiquitin Ligase, Plays an Essential Role in Mitochondrial Quality Control in Parkinson's Disease. Cell Mol. Neurobiol. 41, 1395-1411.
7. Liang, Y., Zhong, G., Ren, M., et al. (2023). The Role of Ubiquitin-Proteasome System and Mitophagy in the Pathogenesis of Parkinson's Disease. Mol. Neurobiol. 60, 6921-6939.
8. Villa, E., Marchetti, S., and Ricci, J.E. (2018). No Parkin Zone: Mitophagy without Parkin. Trends Cell Biol. 28, 882-895.
9. Song, W.H., Yi, Y.J., Sutovsky, M., et al. (2016). Autophagy and ubiquitin-proteasome system contribute to sperm mitophagy after mammalian fertilization. Proc. Natl. Acad. Sci. U. S. A. 113, E5261-E5270.
10. Müller, M., Lu, K., Reichert, A.S., et al. (2015). Synthetic Quantitative Array Technology Identifies the Ubp3-Bre5 Deubiquitinase Complex as a Negative Regulator of Mitophagy. Cell Rep. 10, 1215-1225.
11. Bartel, B., Wunning, I., and Varshavsky, A. (1990). The recognition component of the N-end rule pathway. EMBO J. 9, 3179-3189.
12. Pan, M., Zheng, Q., Yu, T., et al. (2021). Structural insights into Ubr1-mediated N-

degron polyubiquitination. Nature. 600, 334-338.

13. Heck, J.W., Cheung, S.K. and Hampton, R.Y. (2010). Cytoplasmic protein quality control degradation mediated by parallel actions of the E3 ubiquitin ligases Ubr1 and San1. Proc. Natl. Acad. Sci. U. S. A. 107, 1106-1111.
14. Xia, Z., Turner, G.C., Hwang, C.S., et al. (2008). Amino acids induce peptide uptake via accelerated degradation of CUP9, the transcriptional repressor of the PTR2 peptide transporter. J. Biol. Chem. 283, 28958-28968.
15. Du, F., Navarro-Garcia, F., Xia, Z., Tasaki, T. & Varshavsky, A. (2002). Pairs of dipeptides synergistically activate the binding of substrate by ubiquitin ligase through dissociation of its autoinhibitory domain. Proc. Natl. Acad. Sci. U. S. A. 99, 14110-14115.
16. Tasaki, T & Kwon, Y. (2020). The mammalian N-end rule pathway: new insights into its components and physiological roles. Trends Biochem Sci. 32, 520-528.
17. Singh, A., Vashistha, N., Heck, J., et al. (2020). Direct involvement of Hsp70 ATP hydrolysis in Ubr1-dependent quality control. Mol. Biol. Cell. 31, 2669-2686.
18. Hasson, S.A., Kane, L.A., Yamano, K., et al. (2013). High-content genome-wide RNAi screens identify regulators of parkin upstream of mitophagy. Nature. 504, 291-295.
19. Song, T., Yin, F.Q., Wang, Z.Q., et al. (2023). Hsp70-Bim interaction facilitates mitophagy by recruiting parkin and TOMM20 into a complex. Cell. Mol. Biol. Lett. 28, 46-64.
20. Sarraf, S.A., Raman, M., Guarani-Pereira, V., et al. (2013). Landscape of the parkin-dependent ubiquitylome in response to mitochondrial depolarization. Nature. 496, 372-376.
21. Wilfling, F., Lee, C.W., Erdmann, P., Zheng, Y. & Baumeister, W. (2020). A selective autophagy pathway for phase separated endocytic protein deposits. Mol Cell. 80, 764-778.e7.
22. Bodnar, N.O. & Rapoport, T.A. (2017). Molecular mechanism of substrate processing by the Cdc48 ATPase complex. Cell. 169, 722-735.
23. Kim, J.G, Shin, H.C., Seo, T., et al. (2021). Signaling pathways regulated by UBR box-containing E3 ligases. Int. J. Mol. Sci. 22, 8323-8346.
24. Wen, W., Liu, W., Shao, Y., and Chen, L. (2014). VER-155008, a small molecule inhibitor of Hsp70 with potent anti-cancer activity on lung cancer cell lines. Exp. Biol. Med. 239, 638-645.
25. Wang, Z.Q., Zhang, H., Li, X., et al. (2023). Exploiting the "Hot-Spots" of Hsp70-Bim Protein-Protein Interaction to Optimize the 1-Oxo-1H-phenalene-2,3-dicarbonitrile Analogues as Specific Hsp70-Bim Inhibitors. J. Med. Chem. 66, 16377-16387.
26. Li, X., Srinivasan, S.R., Connarn, J., et al. (2013). Analogues of the allosteric heat shock protein 70 (Hsp70) inhibitor, MKT-077, as anti-cancer agents. Acs Med. Chem. Lett. 4, 1042-1047.
27. Liu, C., Lou, W., Zhu, Y., et al. (2018). Proteostasis by STUB1/HSP70 complex controls sensitivity to androgen receptor targeted therapy in advanced prostate cancer. Nat. Commun. 9, 4700.

28. Sukalo, M., Farrer, M.J., Zenker, M., et al. (2014). Mutations in the Human UBR1 Gene and the Associated Phenotypic Spectrum. Hum. Mutat. 35, 521-531.
29. Dauer, W & Przedborski, S. (2003). Parkinson's disease: mechanisms and models. Neuron. 39, 889-909.
30. Zhang, T., Zhang, Y., Cui, M., et al. (2020). The E3 ligase UBR2 regulates cell death under caspase deficiency via Erk/MAPK pathway. Cell Death Dis. 11, 1041.
31. Kim, M.J., Lee, Y.K., Park, K.C., et al. (2021). The Antipsychotic Drug Clozapine Suppresses the RGS4 Polyubiquitylation and Proteasomal Degradation Mediated by the Arg/N-Degron Pathway. Neurotherapeutics. 18, 1768-1782.
32. Tan, T., Zimmermann, M., and Reichert, A.S. (2016). Controlling quality and amount of mitochondria by mitophagy: insights into the role of ubiquitination and deubiquitination. Biol. Chem. 397, 637-647.
33. Pereira, C., Costa, V., Martins, L.M., and Saraiva, L. (2015). A yeast model of the Parkinson's disease-associated protein Parkin. Exp. Cell Res. 333, 73-79.
34. Zhang, Y., Lin, S., Peng, J., et al. (2022). Amelioration of hepatic steatosis by dietary essential amino acid-induced ubiquitination. Mol Cell. 82, 1528-1542.
35. Lunati, A., Lesage, S., and Brice, A. (2018). The genetic landscape of Parkinson's disease. Rev. Neurol. (Paris). 174, 628-643.
36. Gui, Y., Xu, Z., Wang, X., et al. (2021). Enrichment of Rare Variants in E3 Ubiquitin Ligase Genes in Early Onset Parkinson's Disease. Front. Aging Neurosci. 13, 650222.
37. Yuan, L., Wang, Y., Margulis, B.A., et al. (2023). Ectopic BH3-only protein Bim associates with Hsp70 to regulate yeast mitophagy. Dokl Biochem Biophys. 512, 291-298.
38. Wang, Y., Hu, Z., Jiang. M., et al. (2024). Yeast Bxi1/Ybh3 mediates conserved mitophagy and apoptosis in yeast and mammalian cells: convergence in Bcl-2 family. Biol Chem. 405, 417-426.
39. Wang T, Lander ES, Sabatini DM. Large-Scale Single Guide RNA Library Construction and Use for CRISPR-Cas9-Based Genetic Screens. Cold Spring Harb Protoc. 3, pdb.top086892.
40. Hryc, C., Mallampalli, V., Bovshik, E. I., et al. Structural insights into cardiolipin replacement by phosphatidylglycerol in a cardiolipin-lacking yeast respiratory supercomplex. Nat. Commun. 14, 2783-2796.
41. Lazarou, M., Sliter, D.A., Kane, L.A., et al. (2015). The ubiquitin kinase PINK1 recruits autophagy receptors to induce mitophagy, Nature. 524, 309-314.

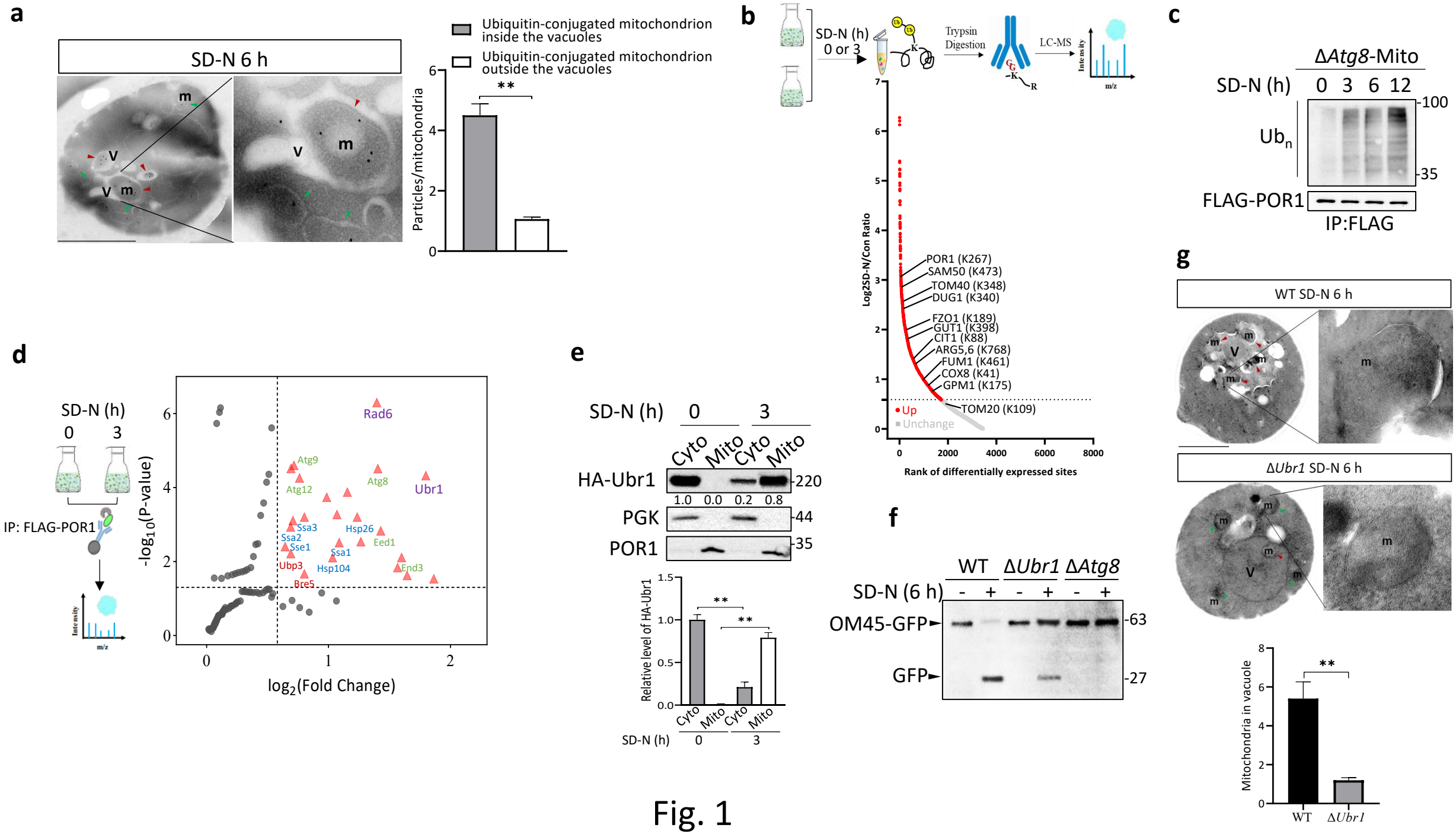
a
SD-N 6 h
m
V
V m
V
m
Ubiquitin-conjugated mitochondrion inside the vacuoles
Ubiquitin-conjugated mitochondrion outside the vacuoles
Particles/mitochondria
**
b
SD-N (h)
0 or 3
Trypsin Digestion
LC-MS
Intensity
m/z
Log2SD-N/Con Ratio
POR1 (K267)
SAM50 (K473)
TOM40 (K348)
DUG1 (K340)
FZO1 (K189)
GUT1 (K398)
CIT1 (K88)
ARG5,6 (K768)
FUM1 (K461)
COX8 (K41)
GPM1 (K175)
TOM20 (K109)
Up
Unchange
Rank of differentially expressed sites
c
ΔAtg8-Mito
SD-N (h) 0 3 6 12
Ubn
100
35
FLAG-POR1
IP:FLAG
d
SD-N (h)
0 3
IP: FLAG-POR1
Intensity
m/z
-log10(P-value)
log2(Fold Change)
Rad6
Atg9
Atg8
Atg12
Ubr1
Ssa3
Hsp26
Ssa2
Sse1
Eed1
Ssa1
Ubp3
Hsp104
End3
Bre5
e
SD-N (h) 0 3
Cyto Mito Cyto Mito
HA-Ubr1
220
1.0 0.0 0.2 0.8
PGK
44
POR1
35
Relative level of HA-Ubr1
**
**
Cyto Mito Cyto Mito
SD-N (h) 0 3
f
WT ΔUbr1 ΔAtg8
SD-N (6 h) - + - + - +
OM45-GFP
63
GFP
27
g
WT SD-N 6 h
m
V
ΔUbr1 SD-N 6 h
Mitochondria in vacuole
**
WT
ΔUbr1

Fig. 1

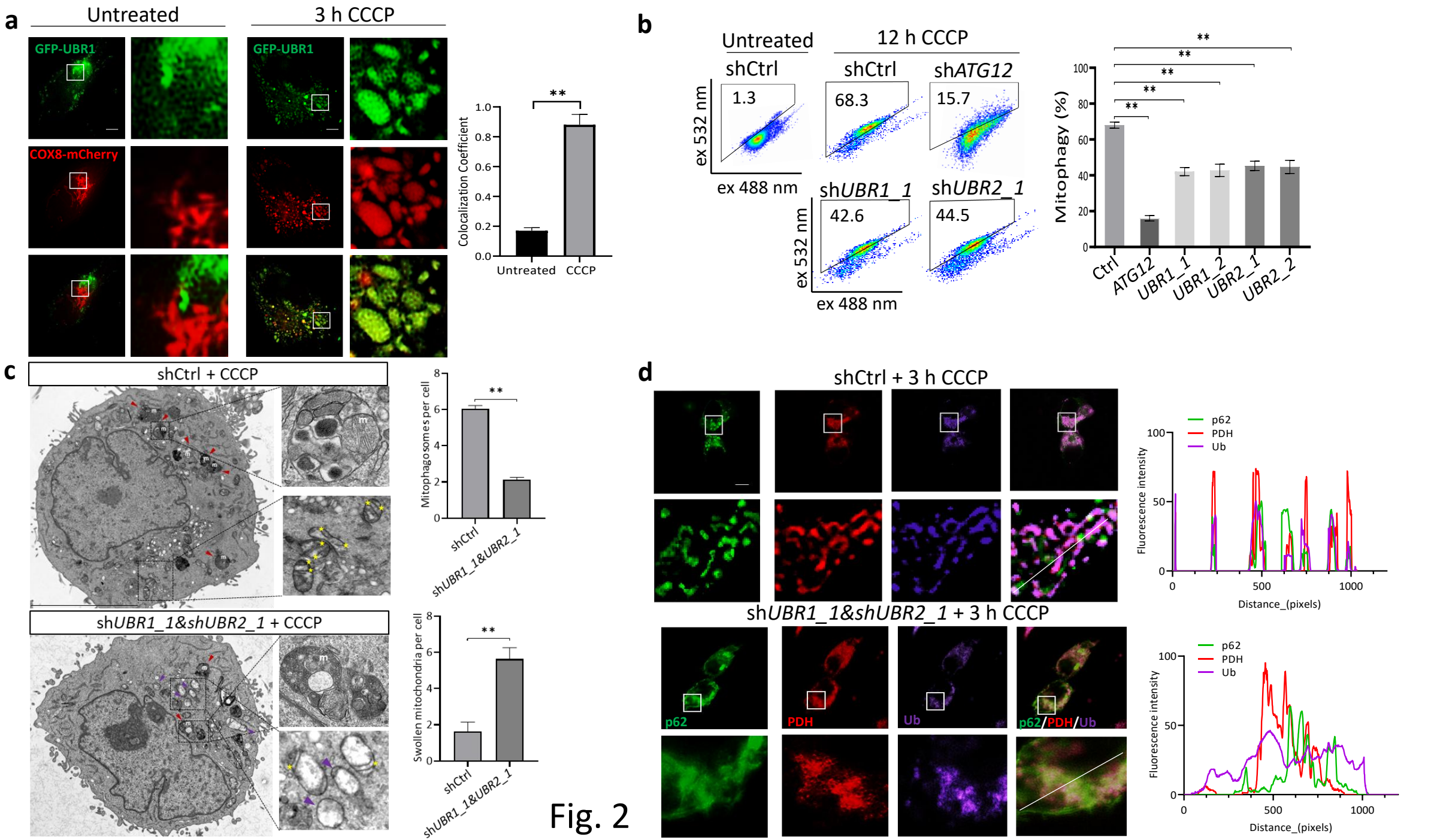
a
Untreated
3 h CCCP
GFP-UBR1
COX8-mCherry
Colocalization Coefficient
Untreated
CCCP
b
Untreated
12 h CCCP
shCtrl
shATG12
shUBR1_1
shUBR2_1
ex 532 nm
ex 488 nm
1.3
68.3
15.7
42.6
44.5
Mitophagy (%)
Ctrl
ATG12
UBR1_1
UBR1_2
UBR2_1
UBR2_2
c
shCtrl + CCCP
shUBR1_1&shUBR2_1 + CCCP
Mitophagosomes per cell
Swollen mitochondria per cell
shCtrl
shUBR1_1&UBR2_1
d
shCtrl + 3 h CCCP
shUBR1_1&shUBR2_1 + 3 h CCCP
p62
PDH
Ub
p62/PDH/Ub
Fluorescence intensity
Distance_(pixels)

Fig. 2

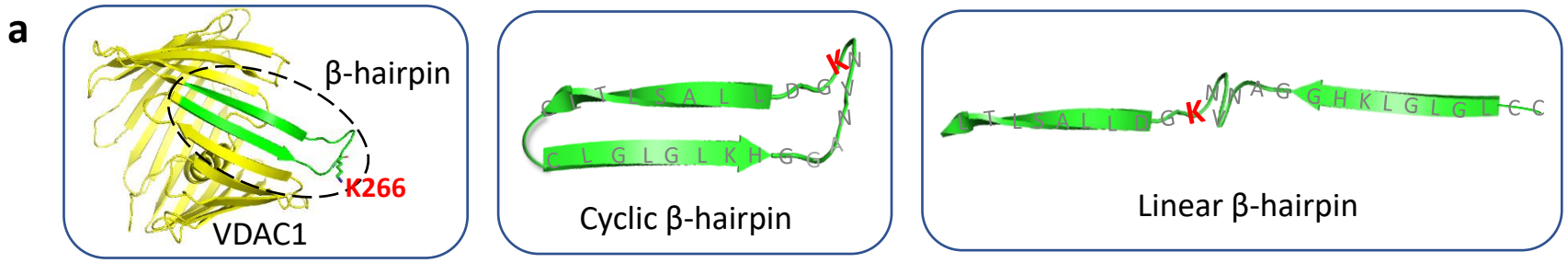

	Hsp70	Ubr1	Hsp70/Ubr1
VDAC1	5.06[a]	11.42[a]	0.38[a]
Cyclic β-hairpin	6.35[a]	7.58[a]	0.64[a]
Linear β-hairpin	no binding[a]	no binding[a]	no binding[a]
Ubr1	0.95[a], 0.78[b]		

[a] K_d value determined by isothermal titration calorimetry (ITC)
[b] K_d value determined by biolayer interferometry (BLI)

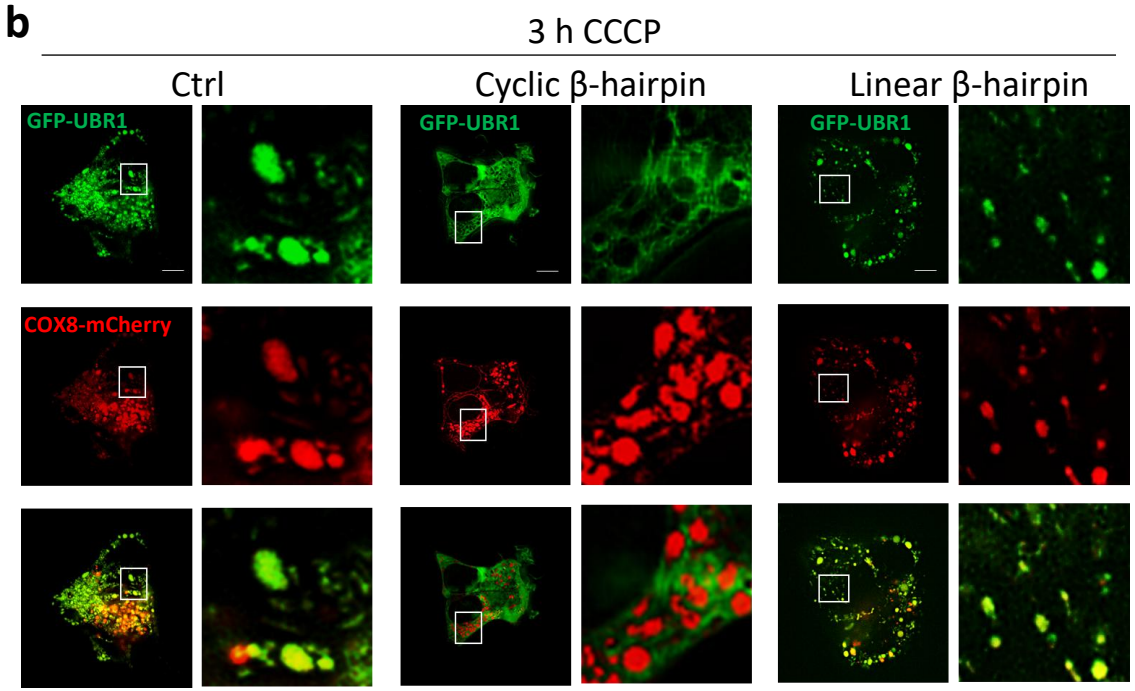

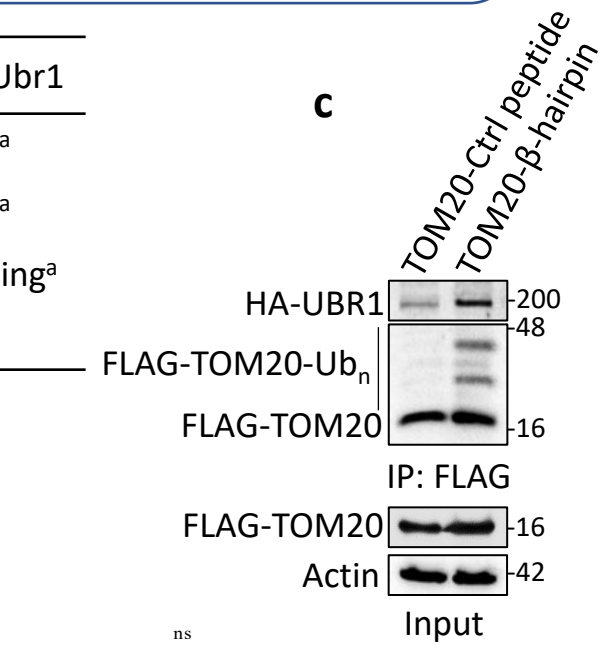

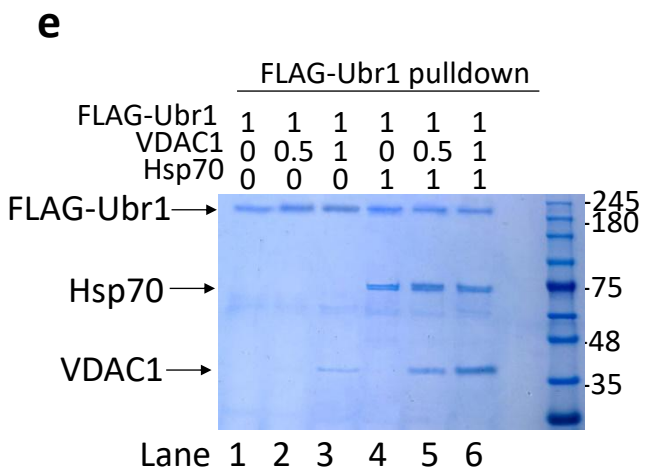

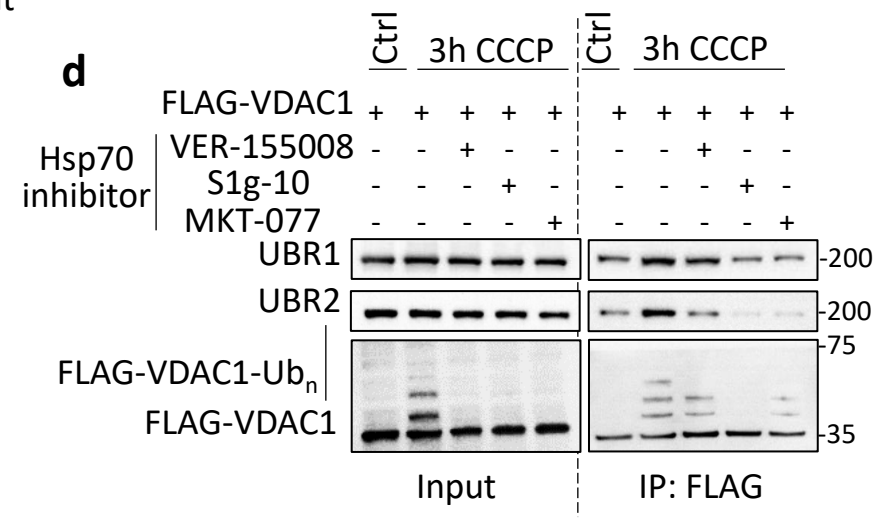

Fig. 3

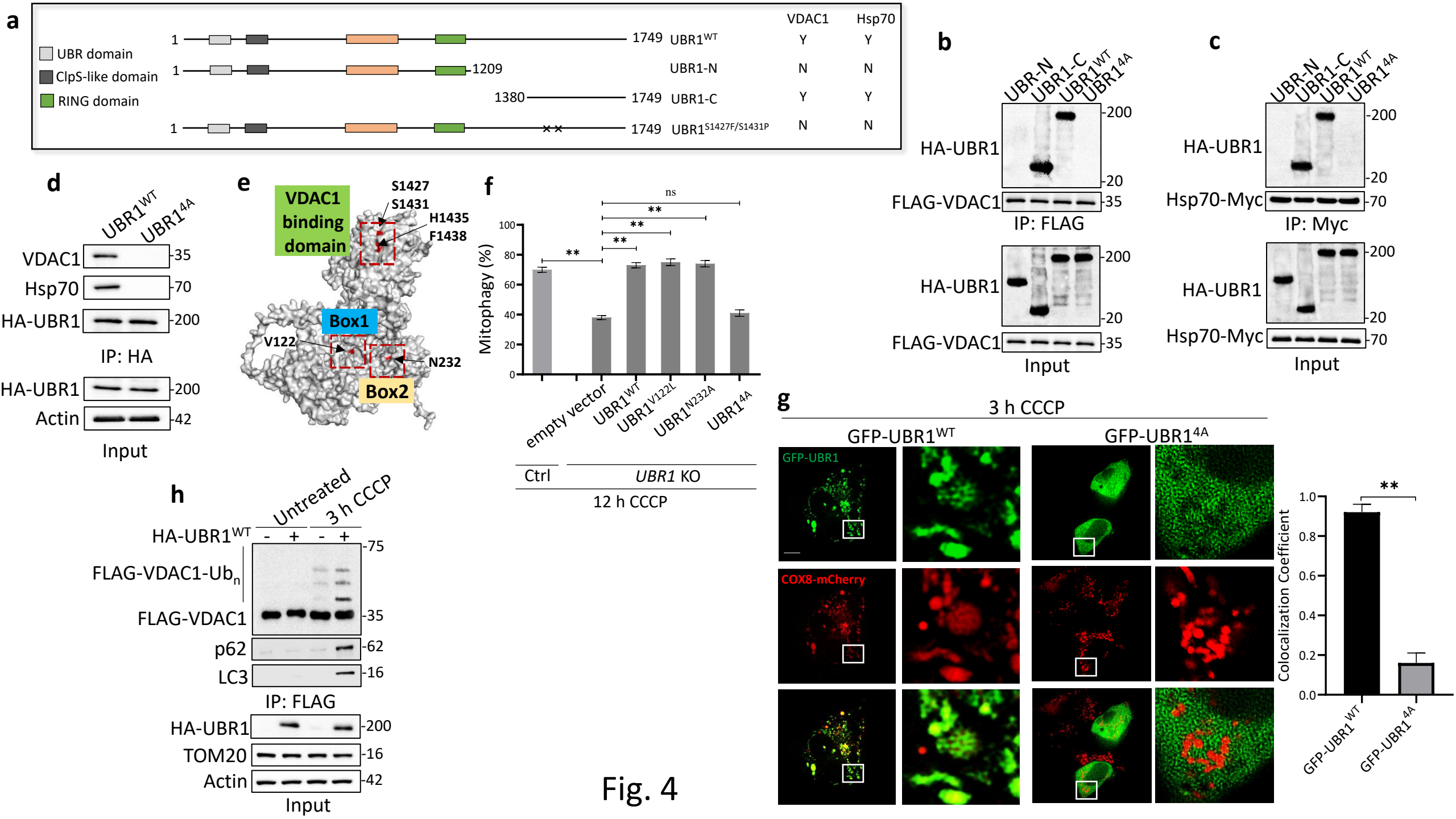
a
UBR domain
ClpS-like domain
RING domain
VDAC1
Hsp70
1
1749
UBR1WT
Y
Y
1
1209
UBR1-N
N
N
1380
1749
UBR1-C
Y
Y
1
1749
UBR1S1427F/S1431P
N
N
b
UBR-N
UBR1-C
UBR1WT
UBR14A
HA-UBR1
FLAG-VDAC1
IP: FLAG
Input
c
HA-UBR1
Hsp70-Myc
IP: Myc
Input
d
UBR1WT
UBR14A
VDAC1
Hsp70
HA-UBR1
IP: HA
Actin
Input
e
VDAC1 binding domain
S1427
S1431
H1435
F1438
Box1
V122
N232
Box2
f
Mitophagy (%)
ns
empty vector
UBR1WT
UBR1V122L
UBR1N232A
UBR14A
Ctrl
UBR1 KO
12 h CCCP
g
3 h CCCP
GFP-UBR1WT
GFP-UBR14A
GFP-UBR1
COX8-mCherry
Colocalization Coefficient
h
Untreated
3 h CCCP
HA-UBR1WT
FLAG-VDAC1-Ubn
FLAG-VDAC1
p62
LC3
IP: FLAG
TOM20
Actin
Input

Fig. 4

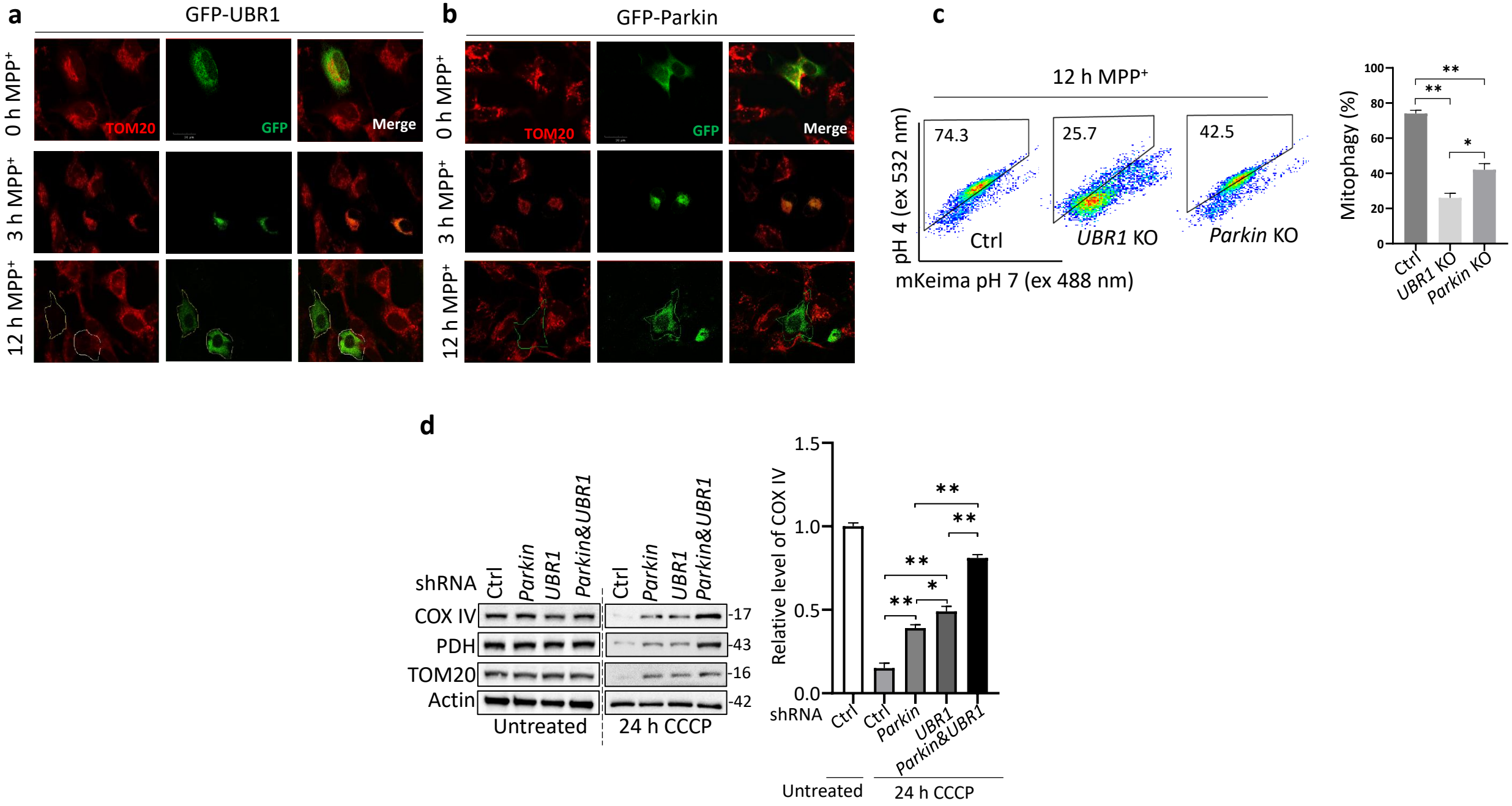
a
GFP-UBR1
0 h MPP+
3 h MPP+
12 h MPP+
TOM20
GFP
Merge
b
GFP-Parkin
c
12 h MPP+
74.3
25.7
42.5
pH 4 (ex 532 nm)
mKeima pH 7 (ex 488 nm)
Ctrl
UBR1 KO
Parkin KO
Mitophagy (%)
d
shRNA
Ctrl
Parkin
UBR1
Parkin&UBR1
COX IV
PDH
TOM20
Actin
-17
-43
-16
-42
Untreated
24 h CCCP
Relative level of COX IV

Fig. 5

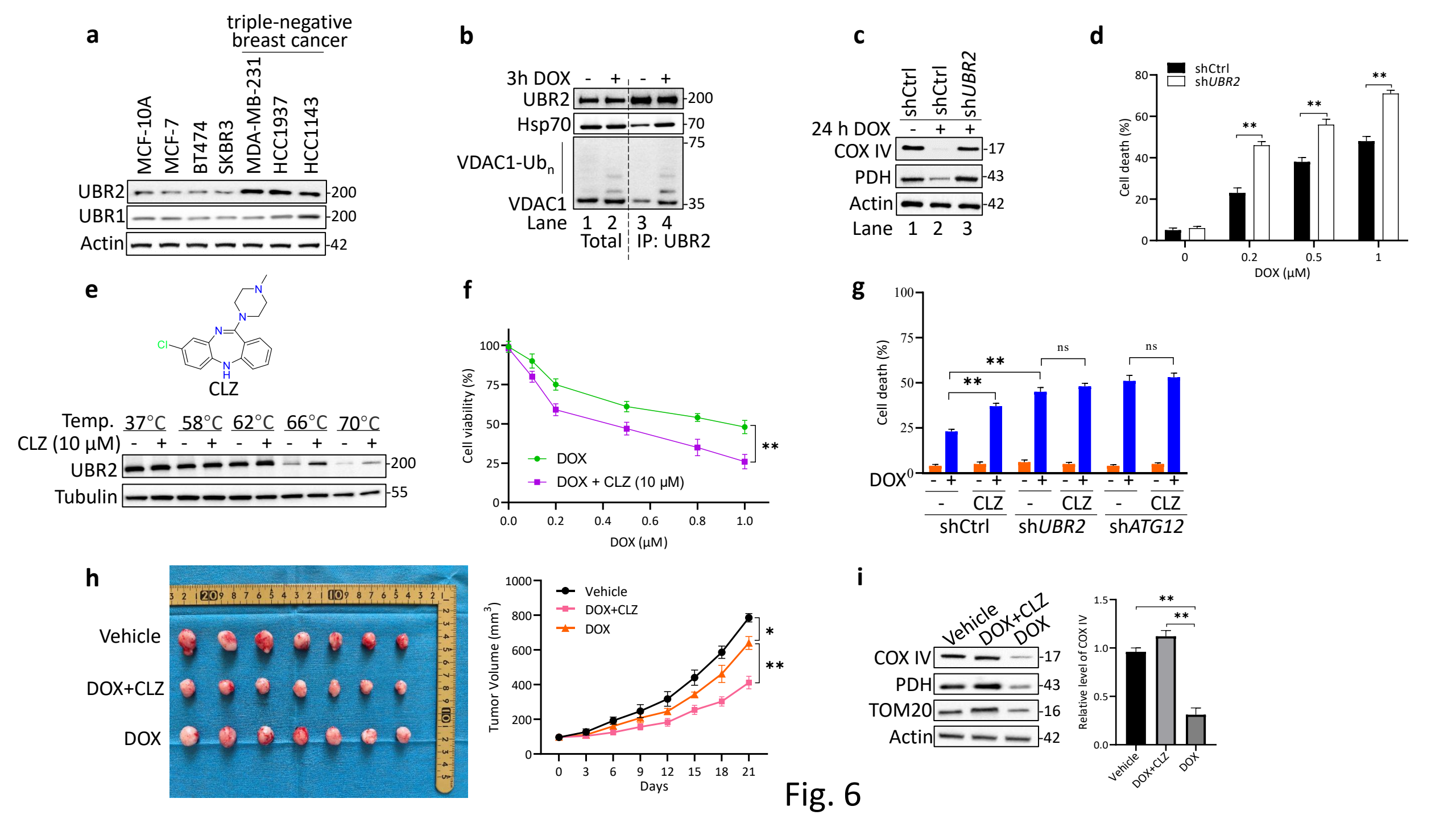
a
triple-negative breast cancer
MCF-10A
MCF-7
BT474
SKBR3
MDA-MB-231
HCC1937
HCC1143
UBR2
UBR1
Actin
200
200
42
b
3h DOX - + - +
UBR2
Hsp70
VDAC1-Ub$_n$
VDAC1
200
70
75
35
Lane 1 2 3 4
Total
IP: UBR2
c
shCtrl
shCtrl
shUBR2
24 h DOX - + +
COX IV
PDH
Actin
17
43
42
Lane 1 2 3
d
shCtrl
shUBR2
Cell death (%)
DOX (μM)
0
0.2
0.5
1
e
CLZ
Temp. 37°C 58°C 62°C 66°C 70°C
CLZ (10 μM) - + - + - + - + - +
UBR2
Tubulin
200
55
f
Cell viability (%)
DOX
DOX + CLZ (10 μM)
DOX (μM)
g
Cell death (%)
DOX
shCtrl
shUBR2
shATG12
CLZ
ns
h
Vehicle
DOX+CLZ
DOX
Tumor Volume (mm^3)
Days
i
Vehicle
DOX+CLZ
DOX
COX IV
PDH
TOM20
Actin
17
43
16
42
Relative level of COX IV

Fig. 6


a
Ubr1
Ub
Hsp70
LC3
KUb
Ub
Ub
VDAC1
p62
b
Yeast
Ubr1
Mitophagy
Mammalian
Parkin
UBR1/2
Mitophagy

Fig. 7